# Broadband mean free path of diffuse light in polydisperse ensembles of scatterers for white light-emitting diode lighting

Willem L. Vos,[1,*] Teus W. Tukker,[2] Allard P. Mosk,[1] Ad Lagendijk,[1,3] and Wilbert L. IJzerman[4]

[1]Complex Photonic Systems (COPS), MESA+ Institute for Nanotechnology, University of Twente, P.O. Box 217, Enschede 7500 AE, The Netherlands

[2]Philips Lighting—Light Sources and Electronics, Mathildelaan 1, Eindhoven 5611 BD, The Netherlands

[3]FOM-Institute for Atomic and Molecular Physics (AMOLF), Amsterdam 1098 XG, The Netherlands

[4]Philips Lighting—Optics, Mathildelaan 1, Eindhoven 5611 BD, The Netherlands

*Corresponding author: w.l.vos@utwente.nl

Received 13 November 2012; revised 1 February 2013; accepted 8 February 2013; posted 8 February 2013 (Doc. ID 179728); published 15 April 2013

We study the diffuse transport of light through polymer slabs containing $TiO_2$ scattering particles. The slabs are diffuser plates typical of a commercial white light-emitting diode (LED) module (Fortimo). We have measured the diffuse transmission and reflection properties over a broad wavelength range (470–840 nm) from which we derive the transport mean free path using the theory of light diffusion. With increasing scatterer density, the mean free path becomes shorter. The mean free path increases with wavelength; hence, blue light is scattered more strongly than red light. To interpret the results, we propose an *ab initio* model without adjustable parameters for the mean free path by using Mie theory. We include inhomogeneous broadening as a result of the size distribution of the scattering particles as measured by dynamic light scattering. Surprisingly, the calculated mean free path decreases with wavelength, at variance with our experiments, which is caused by particles with radii $R$ in excess of 0.25 μm. Close inspection of the scatterers by electron microscopy reveals that large particles ($R > 0.4$ μm) consist of clusters of small particles ($R < 0.13$ μm). Therefore, we have improved our model by only taking into account the individual scatterers within the clusters. This model predicts mean free paths in good agreement with our experimental results. We discuss consequences of our results to white LED lighting modules. 

*OCIS codes:* (160.4236) Nanomaterials; (230.3670) Light-emitting diodes; (290.4020) Mie theory; (290.4210) Multiple scattering; (290.5850) Scattering, particles; (290.7050) Turbid media.

http://dx.doi.org/10.1364/AO.52.002602

## 1. Introduction

There is a strong worldwide drive to efficiently generate white light for many applications in lighting. A modern approach is to employ white light-emitting diodes (LEDs) [1–4]. These white LEDs typically consist of a blue semiconductor diode combined with luminescent phosphors that convert part of the blue light to the additional colors yellow, green, and red. In state-of-the art white-light LED technology, one exploits the light-scattering properties of the phosphors. Thanks to intentional structural features such as air inclusions or material scatterers, light is multiply scattered [3,4]. Consequently, the transport of light becomes diffusive, which is helpful to obtain an even lighting without hot spots or without angular color distribution, as is desired for

1559-128X/13/122602-08$15.00/0

lighting applications. Moreover, photons are recycled so that thin phosphor layers can be used. Thereby, cost efficiency is improved and the environmental impact is reduced.

Central challenges in understanding the optical properties of white LEDs arise from limitations in the physical understanding of the combined multiple light scattering and energy conversion in phosphors. The properties of the LEDs are currently described by models wherein light scattering and energy conversion are treated by ray-tracing and Monte Carlo techniques [4–6]. Unfortunately, it appears that the LED spectra cannot be predicted quantitatively, or that relevant optical parameters must be adjusted to match with measured data [7,8]. These limitations in predictive power clearly hamper the design and development of efficient white LEDs with desired characteristics or with novel tailored properties.

An improved description of multiple light scattering can be obtained by analytical theories originating from nanophotonics, wherein multiple scattering of light is described from first principles [9–12]. The advantage of such *ab initio* models over ray tracing is that one obtains fundamental physical insight, starting from the detailed nanostructure of a sample. Moreover, calculating optical properties from a model is computationally much faster than performing a ray tracing simulation. On the other hand, we note that such models are usually limited to simple sample geometries, such as a slab, a sphere, or a semi-infinite medium. To ultimately model complex LED luminaires that are of practical interest, one must resort to ray-tracing models that are improved with the aid of *ab initio* models.

Most nanophotonic theories and experiments to date are applied to situations where narrowband light sources have been used. Therefore the main question arises of how to extend nanophotonic models to describe the transport for broadband light, which is particularly relevant to white LEDs. There have been a few pioneering broadband studies, on dense Si powder in the infrared [13], on dense resonant photonic glasses [14], and on dense $TiO_2$ powder [15]. As a first step in applying nanophotonics to white LEDs, the aim of the present paper is to obtain an understanding of the broadband multiple light scattering of diffuser slabs typical of white LEDs. To this end, we have chosen to study the diffuser plates of commercially available white LED luminaires [16] by total transmission, also known as diffuse transmission, which is the transmission integrated over all outgoing angles at which light exits from a medium. The total transmission contains information on the transport mean free path, a crucial parameter that describes multiple scattering of light [9–12,17]. The transport mean free path is the distance it takes for the direction of light to become randomized while light performs a random walk in a scattering medium. To model the results, we use the well-known Mie theory, supplemented by the size distribution of the scatterers.

## 2. Experimental Details

In this paper, we present results obtained on five polymer slabs (polycarbonate, Teijin Panlite ML2102 [18]) typical for Fortimo white LED units [16]. In order to scatter light, the polymer slabs contain $TiO_2$ particles [19] with weight densities ranging through $\phi = 0$, 0.01, 0.05, 0.10, and 1.0 wt. %. For subsequent modeling, the mass density is converted to a scatterer volume fraction $f$ by a conversion factor of 0.3 vol. %/wt. %, which takes into account the densities of the materials. Similar results were obtained on other slabs made from different polymers. The slabs were fabricated as follows: a powder of $TiO_2$ particles is mixed with the polymer by making a compound in the required weight ratio. Next, the compound is shaped into disks (60 mm × 2 mm) by industrial injection molding. The disks have a thickness $L = 2.0$ mm.

The $TiO_2$ particles were commercially obtained from Kronos (Germany). A scanning electron micrograph (SEM) of the particles is shown in Fig. 1. The particles reveal a large variation of sizes, similar to our earlier experience with $TiO_2$ powders [20]. The broad size distribution is favorable for a uniform scattering of white light [1]. The inset shows a close up of a large particle with a radius $R = 0.45$ μm that reveals that it consists of a cluster of smaller particles with radii in the range up to about 0.13 μm.

The size distribution of similar scatters is shown in Fig. 2. The radii are determined by dynamic light scattering, at Philips MiPlaza, which yields a hydrodynamic radius [21]; while such a radius is slightly larger than the one determined from SEM, this effect is minor compared to the very broad distribution. Anticipating the fact that for the model calculations the particles have to be of spherical shape, the size distribution has been obtained by adopting this simplification. As will be explained later this is not a serious shortcoming of our approach. The distribution has a broad and asymmetric peak with a maximum at a particle radius $R = 0.14$ μm, followed by a

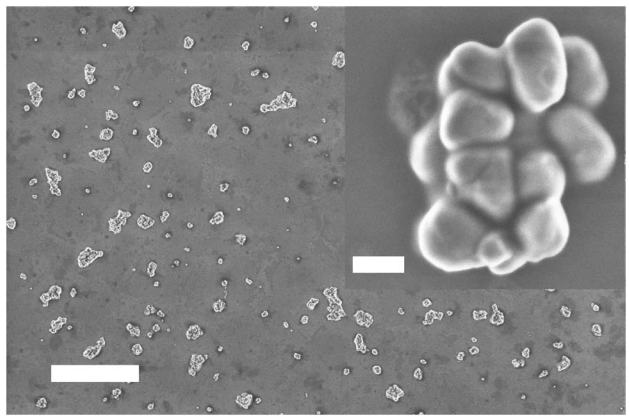

Fig. 1. SEM of $TiO_2$ particles as used in the experiments. The scale bar is 10 μm long. The image shows a large variation in sizes as illustrated in Fig. 2. Inset: zoom-in of a large particle that consists of a cluster of smaller particles ($R < 0.13$ μm); scale bar is 0.2 μm long.

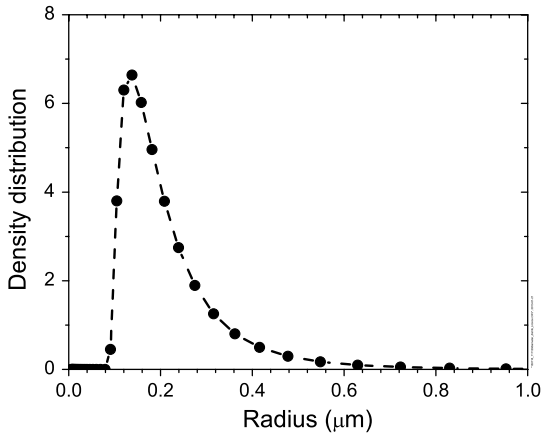


Fig. 2. Distribution of the radii $n(R)$ of the $TiO_2$ light scattering particles used in the experiments. Since the distribution is obtained from dynamic light scattering, the radii are hydrodynamic radii [21]. The particles are approximated to be spherical, and the distribution is normalized to 1.

broad tail of large particles up to $R = 1.0$ μm. In this distribution of hydrodynamic radii, no provision could be made for small particles within a cluster.

To measure broadband, spectrally resolved, total transmission $T$ of light we used a setup using a supercontinuum white-light source (Fianium SC-450-2). The incident light was filtered with a 850 nm short pass filter to remove long wavelengths, notably the bright 1064 nm pump light from the source. The beam was collimated and the diameter was set by several irises to less than 2 mm, and was incident at normal incidence on a slab that was horizontally placed on the entrance port of an integrating sphere. Since the incident beam was not focused, we can safely neglect the dependence of total transmission on the angle of incidence. We verified that the entrance port of the integrating sphere was sufficiently large to accept the complete diffuse spot emanating from the strongest scattering sample. The diffuse output of the integrating sphere was monitored with a fiber-to-chip spectrometer (Avantes) with a spectral resolution of 1.2 nm. The spectral range runs from $\lambda = 470$ to 840 nm, and is limited by the white light source output and the cutoff wavelength of the filter.

For all slabs, we collected several spectra and repositioned a sample in between scans to test the reproducibility and sample homogeneity; moreover, the measurements reproduced to within a few percent on different days. To calibrate the total transmission values, we collected reference spectra in absence of a sample, and determined the total transmission as the ratio of a sample spectrum and a reference spectrum. Reference spectra were frequently collected in between sample spectrum measurements to correct for possible time-dependent changes in the setup. This calibration procedure results in a relative reproducibility better than 1%, between 480 and 830 nm. The total relative error in the transmission is estimated to be about 5% (percent points, including systematic errors) based on the variations between different measurements.

Both the diffuse reflectivity and the total reflectivity—equal to the sum of the diffuse and the specular reflectivities—were acquired at the Light Labs on the same samples, using a Varian Cary 5 spectrometer with an accuracy of 1% in the wavelength range between 360 and 800 nm. From the total reflectivity and the diffuse reflectivity, we obtained the specular reflectivity $R_s$ by straightforward subtraction.

## 3. Results

In Fig. 3, we show total transmission spectra for slabs with increasing $TiO_2$ content. In broad terms, such spectra are a measure for the degree of light scattering: less total transmission means more scattering. Comparing spectra with increasing $TiO_2$ content, we observe a decreasing total transmission, which is intuitively sensible as the scattering strength is expected to increase with the density of scatterers. In each spectrum, the transmission increases with wavelength, indicating more scattering for blue than for red light, which is also intuitively reasonable. The weak, fringe-like features between 550 and 600 nm are artifacts from the setup that could not completely be removed by referencing. The faint features near 600 and 676 nm are caused by absorption of the polymer matrix as concluded from additional experiments [22]; since they are not important to the main results of this paper, they will henceforth be disregarded. The sample without additional scatterers has a total transmission between 70% and 75%, which appear to be the limiting values for weakly scattering media as we will discuss below.

According to diffusion theory for light in complex media [9–12,17], the total transmission $T(\lambda)$ of a scattering medium is given by the following expression:

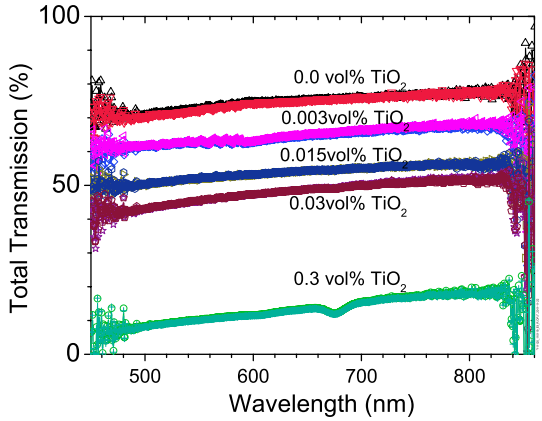


Fig. 3. Total transmission $T$ versus wavelength of polymer slabs with increasing $TiO_2$ particle density (indicated), from top to bottom: $f = 0$ vol. % (black and red symbols), 0.003 vol. % (blue and magenta symbols), 0.015 vol. % (dark yellow and navy symbols), 0.03 vol. % (purple and wine symbols), 0.3 vol. % (olive and dark cyan symbols). For each sample two different measurements are shown, indicating the good reproducibility.

$$T(\lambda) = (1 - R_s(\lambda)) \frac{\ell(\lambda) + z_e(\lambda)}{L + 2z_e(\lambda)}. \quad (1)$$

The total transmission is inversely proportional to the sample thickness $L$, and can thus be interpreted as the optical analogue of Ohm's law for the conductance of electrons. Furthermore, $R_s(\lambda)$ is the specular reflectivity of the incident light beam from the front face, and $z_e(\lambda)$ is the extrapolation length that describes the boundary conditions of the diffuse intensity at the interface of the sample. Last but not least, $\ell(\lambda)$ is the transport mean free path we wish to study.

Since the mean free path of light in our samples will appear to be comparable to the sample thickness ($\ell \simeq L$), in other words the samples are moderately in the multiple scattering regime, it is relevant to wonder if it is justified to invoke diffusion theory. In [23], the enhanced backscattering cone, a quintessential multiple scattering phenomenon, was calculated both with exact theory and with diffusion theory. It appears that even for low order of scattering, i.e., for weak multiple scattering, the diffusion theory agrees very well (better than 10%) with the exact results. In addition, Durian has concluded from simulations of the diffuse transmission of samples with widely varying thickness that the diffusion approximation is in surprisingly good agreement with the exact results, even for a sample thickness of the order of the mean free path [17]. Therefore, we conclude that it is justified to apply diffusion theory to our samples.

To obtain the mean free path from the diffuse transmission through Eq. (1), we have measured the specular reflectivity $R_s(\lambda)$ of the incident beam on the samples, shown in Fig. 4. The sample with the highest $TiO_2$ particle density reveals a shallow trough near 400 nm, which agrees with the intrinsic absorption of $TiO_2$ [24,25]. It is remarkable that the spectra of all samples closely coincide: they start at a reflectivity of 5% in the blue and decrease to 4% in the red. The specular reflectivity is, in contrast to the diffuse reflectivity, mostly determined by the optical properties of the polymer and nearly independent of the density of $TiO_2$ scatterers in the slabs. This dependence is reasonable since the volume fraction of the scatterers ($f \leq 0.3\%$) is much less than of the polymer and as a result the $TiO_2$ particles hardly contribute to the average index of refraction. Assuming Fresnel reflectivity, the average refractive index of the diffusers decreases from about 1.55 in the blue to 1.5 in the red, in agreement with typical values for polymers.

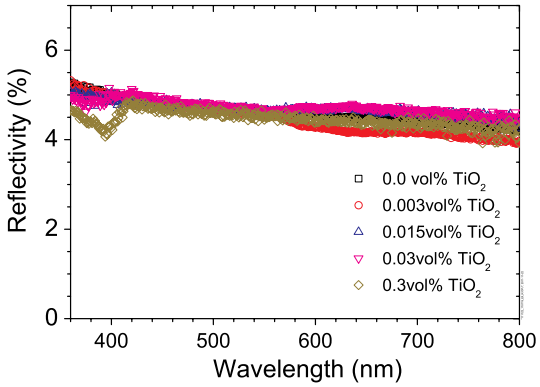


Fig. 4. Reflectivity $R$ versus wavelength of the polymer slabs with increasing $TiO_2$ particle density: $f = 0$ vol. % (black squares), 0.003 vol. % (red circles), 0.015 vol. % (blue triangles), 0.03 vol. % (magenta inverted triangles), and 0.3 vol. % (dark yellow diamonds).

From diffusion theory, one can express the extrapolation length in terms of the mean free path $\ell(\lambda)$ as [26,27]:

$$z_e(\lambda) = \frac{2\ell(\lambda)}{3} \frac{1 + \bar{R}(\lambda)}{1 - \bar{R}(\lambda)}. \quad (2)$$

Here, $\bar{R}(\lambda)$ is the polarization and angle-averaged internal diffuse reflectivity of the sample. For a medium with an average refractive index $n = 1.5$ the average internal diffuse reflectivity is equal to $\bar{R} = 0.57$, and $\bar{R} = 0.6$ for $n = 1.55$ [26,27]. As a result we obtain the transport mean free path from the measured and known quantities as

$$\ell(\lambda) = \frac{L}{t(\lambda)\left(1 + \frac{2}{3} r(\lambda) - \frac{4}{3} \frac{r(\lambda)}{t(\lambda)}\right)}, \quad (3)$$

where the factor $t(\lambda)$ is shorthand notation for a ratio including total transmission and specular reflectivity:

$$t(\lambda) \equiv \frac{[1 - R_s(\lambda)]}{T(\lambda)} = \frac{L + 2z_e(\lambda)}{\ell(\lambda) + z_e(\lambda)}, \quad (4)$$

and the factor $r(\lambda)$ includes the angle-averaged internal diffuse reflectivity $\bar{R}(\lambda)$:

$$r(\lambda) \equiv \frac{1 + \bar{R}(\lambda)}{1 - \bar{R}(\lambda)}. \quad (5)$$

For the samples with low scatterer densities (0 and 0.003 vol. %), the mean paths are much larger than the sample thickness $\ell \gg L$, although the samples have visually a diffuse appearance. If we also use the observation that the specular reflectivity is relatively low ($R_s \ll 1$), we find for the total transmission in this limit that

$$\lim_{(\ell \gg L, R_s \ll 1)} T(\lambda) = \frac{\ell(\lambda) + z_e(\lambda)}{2z_e(\lambda)} = \frac{1 + \frac{2}{3} r}{\frac{4}{3} r}. \quad (6)$$

We draw two conclusions from Eq. (6): first, since the mean free path cancels in numerator and denominator, the total transmission for these weakly scattering samples is independent of the mean free path. Obviously it is in this limit not possible to derive

the mean free path from a total transmission experiment. Secondly, by using $\bar{R} = 0.57$ to 0.60 (see above), $r(\lambda)$ is between 3 and 4, and therefore the total transmission ranges from 69% to 75%, in very good agreement with the results in Fig. 3. Thus, the limiting value for the total transmission is not necessarily 100%, which illustrates that total transmission behaves differently from the usual Lambert–Beer transmission using nondiffuse input and output beams.

The wavelength-dependent mean free paths for optically thick samples with ≥0.015 vol. % obtained from Eq. (3) are summarized in Fig. 5. For the samples with a scatterer density of 0.015 vol. % and higher, the mean free paths are less than the sample thickness of 2 mm. The mean free paths increase with wavelength and decrease with increasing density of $TiO_2$ scatterers as intuitively expected. For the strongest scattering sample, the mean free path increases by a factor 3.5×, from 0.04 to 0.14 mm in the spectral range between 450 and 750 nm. This trend reveals that the observed scattering is not in the Rayleigh regime, as the well-known $\lambda^4$ scaling of the scattering cross section [28–30] would correspond to an increase by a factor of 8, which is not the case here. Therefore, the size parameter $x$ that characterizes the regime of light scattering (defined as $x = 2\pi mR/\lambda$; $m$ is the refractive index contrast to the surrounding medium) is not small as in the Rayleigh regime; in the Discussion section, we will see that $x$ is in the Mie regime [28,29].

To investigate the density dependent behavior of light scattering, we plot in Fig. 6 the inverse mean free path versus the density of $TiO_2$ scatterers in the diffuser plate. At all three wavelenghts shown ($\lambda = 500$, 600, 700 nm) that span the measured range, the inverse mean free path increases linearly with the particle density. This agrees with the results by van der Mark *et al.* [23], who observed a linear relation to 20 vol. %. The deviations from linearity

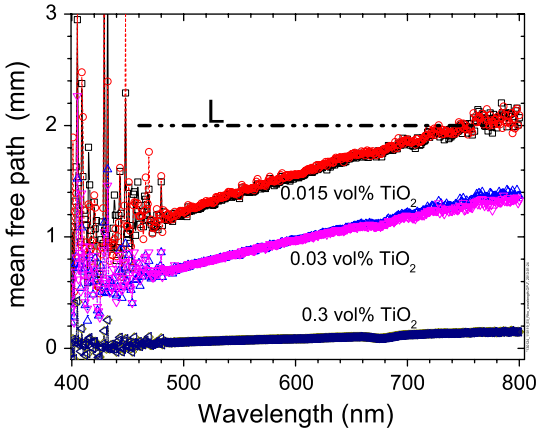


Fig. 5. Transport mean free path $\ell$ versus wavelength for polymer slabs with increasing $TiO_2$ content, from bottom to top: $f = 0.3$ vol. % (dark blue), 0.03 vol. % (magenta), and 0.015 vol. % (red). The horizontal dashed–dotted line illustrates the sample thickness $L$.

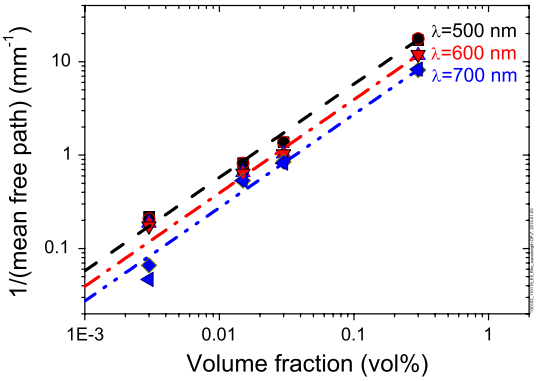


Fig. 6. Inverse of the transport mean free path versus density of $TiO_2$ scatterers in vol. % in a log–log representation. Data are shown for three different wavelengths: $\lambda = 500$ nm in black, 600 nm in red, 700 nm in blue. For each data set, a linear dependence with zero offset is plotted [cf. Eq. (9)] with slope 57.7, 39.4, and 29.4 from top to bottom.

are largest at the lowest density, which is reasonable since here the scatterers affect the total transmission the least so the relative errors are the largest. At densities beyond 0.015 vol. %, the variations in inverse mean free path are less than 0.1, corresponding to a relative error of better than 10%. We conclude that the scatterers are so dilute that the multiple light scattering takes place in the independent scattering approximation [9–12]. This is in agreement with Kubelka–Munk considerations [31], which is helpful as it considerably simplifies the modeling.

## 4. Model

To obtain an analytical model of the mean free path, we use Mie scattering theory [28,29] that is exact for a single particle, combined with the measured distribution $\rho(R)$ of particle radii $R$ as has been measured at Philips. In this section, all mean free paths are implicitly understood to depend on frequency or wavelength $\lambda$. We assume that the particles scatter independently, which is reasonable as the scatterer density is low ($f \leq 0.3$ vol. %) and which is borne out by the results in Fig. 6. Therefore, we add the contributions from all scattering particles to the optical cross sections $C$ (scattering, absorption, or extinction). As discussed earlier, e.g., in [32,33], the inverse scattering mean free path for a discrete distribution of particles is equal to

$$\frac{1}{l_{\text{scat}}} = \frac{N}{V} C_{\text{avg}} = \frac{N}{V} \frac{N_1 C_1 + N_2 C_2 + \cdots + N_m C_m}{N_1 + N_2 + \cdots + N_m}, \quad (7)$$

where $N_i$ is the number of scatterers with cross section $C_i$, and $N/V$ is the number density of scatterers. For a continuous distribution of particle radii, the inverse scattering mean free path can be generalized to

$$\frac{1}{l_{\text{scat}}} = nC_{\text{avg}} = n \frac{\int_0^{R_{\max}} \mathrm{d}R n(R) C(R)}{\int_0^{R_{\max}} \mathrm{d}R n(R)}, \quad (8)$$

where $n(R)$ is the number density of scatterers with radii $R$, and $n \equiv (N/V)$ the total number density of scatterers. Since we wish to interpret the total transmission, we have calculated the transport mean free path $\ell$ averaged over the particle size distribution that is equal to:

$$\frac{1}{\ell} = nC_{\text{avg}}(1 - \langle\cos(\theta)\rangle_{\text{avg}}) = \ldots \tag{9}$$

$$\ldots = n\frac{\int_0^{R_{\max}} \mathrm{d}Rn(R)C(R)(1 - \langle\cos(\theta)\rangle(R))}{\int_0^{R_{\max}} \mathrm{d}Rn(R)}, \tag{10}$$

where $\langle\cos(\theta)\rangle(R)$ is the average scattering angle of scatterers with radii $R$ [28,29], and $\langle\cos(\theta)\rangle_{\text{avg}}$ is the average scattering angle.

## 5. Discussion

Using the model described in the previous section, we have calculated the transport mean free path as a function of wavelength using the known particle size distribution $n(R)$ (see Fig. 2). The calculated mean free paths are shown in Fig. 7 and are compared to the experimental data for the sample with the highest density of scatterers with a volume fraction $f = 0.3$ vol. %. With increasing wavelength, the calculated mean free paths decrease from 1.15 to 0.9 mm. Thus the calculated values differ in two aspects from the experiments: first, the calculated ones are a factor 6–27 times higher than the measured ones, and second, the calculated values decrease with wavelength instead of increasing. The major differences between the model and our observations may be attributed to two main physical reasons:

1. The SEM picture of the $TiO_2$ scatterers in Fig. 1 reveals that the scatterers have shapes that differ from the spherical shape assumed in our model. Nevertheless, it appears that approximating the scatterers by spheres is not a severe limitation in the multiple-scattering limit. Fine details of single-scattering properties are rapidly washed out when the sample contains particles with a substantial size distribution and when multiple scattering sets in. Averaging over a size distribution washes out resonant effects that may occur for a certain shape, and multiple scattering results in an orientational averaging that washes out angle-dependent resonances of nonspherical scatterers (shown for single scattering in, e.g., [33]). Therefore, we consider it unlikely that nonsphericity of the scatterers is the main source of discrepancy between model and observations.

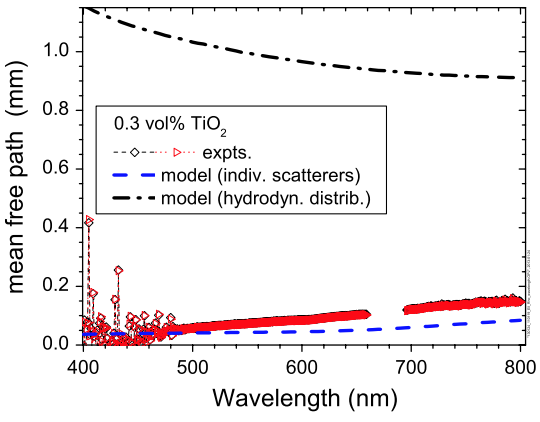


Fig. 7. Transport mean free path $\ell$ versus wavelength. Symbols are our measurements for a Fortimo slab with $f = 0.3$ vol. % $TiO_2$ scatterers. The spurious $\lambda = 676$ nm absorption band has been omitted [22]. The black dashed–dotted curve is calculated for a polydisperse assembly of spherical scatters with a hydrodynamic size distribution (see Fig. 2). The blue drawn curve is calculated for a polydisperse assembly of spherical scatters with a size distribution cutoff at $R = 130$ nm based on the SEM results.

2. The microscopic structure in Fig. 1 also reveals that the large $TiO_2$ scatterers effectively consist of clusters of smaller particles with radii $R < 0.13$ μm. To investigate this hypothesis, we have analyzed the integrals over particle sizes in the numerator and denominator of Eqs. (9) and (10) by calculating the mean free path for an increasing integral boundary $R_{\max}$, in other words, for an increasingly broad size distribution $n(R)$ [34]. We find that only for small spheres up to $R_{\max} = 0.25$ μm does the calculated mean free path have a positive slope with wavelength in agreement with the experimental results. Further increasing the integral boundary $R_{\max}$ results in a reversal of the slope. Such a decrease of $\ell$ versus $\lambda$ is caused by the fact that the larger sphere fractions in the distribution (with radii $R_{\max} > 0.25$ μm) have a size parameter $x > 3$, which means that the scattering cross section is in the range beyond the first main Mie resonance [28,29]. Since the cross section has a maximum at a resonance, it decreases with increasing size parameter, resulting in a decreasing mean free path with wavelength. The fraction of large spheres dominates the results in Fig. 7, which is reasonable since the scattered power increases with scatterer volume squared.

Based on this observation, we propose a second model, based on visual inspection of the SEM pictures, wherein we limit the maximum sphere radius in the distribution of sphere sizes to $R_{\max} = 0.13$ μm; in other words, we cut the distribution shown in Fig. 2 off at $R = 0.13$ μm (we neglect deviations from sphericity of the small scatterers for the same reason as explained above) [34]. The results from this heuristic second model without adjustable parameters are also shown in Fig. 7. The calculated mean free paths range from 0.04 to 0.09 mm, which is in much better agreement with the experimental data (0.04–0.14 mm) than the first model above. The relative difference between experiment and model is less than 35%, which is a substantial improvement over the first model where the differences amount to 600%–2700%. In addition, the slope of mean free path versus wavelength is slightly positive, similar to the experimental results. The dramatically improved

agreement confirms our hypothesis that small particles (also those within the clusters) are the dominant source of scattering. The observation that the calculated mean free paths are somewhat smaller than the measured ones is slightly surprising since in the diffuser plates, light is not only scattered by the $TiO_2$ scatterers, but also by other inhomogeneities, as is evident from the observation that plates without $TiO_2$ scatterers have a milky appearance. A possible cause for the difference may be that the fabrication of the polymer plates by extrusion may be accompanied by strong shear forces that could affect the size distribution, as larger particles might be reduced in size. At any rate, we find the agreement between our second model and the data gratifying in view of three features: (i) we have obtained a first *ab initio* model for multiple light scattering in white LED components, (ii) our model has no freely adjustable parameters, and (iii) it is challenging to derive a size distribution for particles within clusters. Finally, we note that since both the measured inverse mean free path and the modeled ones are proportional to the scatterer density [see Fig. 6 and Eq. (9), respectively], the good agreement between the second model and the data also holds for densities other than $f = 0.3$ vol. %.

Let us place our results in context with previous studies: Rivas *et al.* reported mean free paths on dense Si powder with a very broad size distribution, as measured by total transmission in the infrared [13]. They observed that the mean free path increases with wavelength from 0.6 μm at $\lambda = 1.4$ μm to 0.85 μm at $\lambda = 2.5$ μm, a similar trend as reported here. A model of independently scattering monodisperse Mie-spheres revealed a moderate agreement with many unobserved resonances. Much better agreement was obtained with an advanced model based on the coherent potential approximation (to take into account scatterer–scatterer effects typical of elevated densities), and averaging over the broad size distribution. The agreement between their overall behavior and our results supports our heuristic approach to take dependent scattering into account by limiting the size distribution to the particle sizes within clusters.

Secondly, García *et al.* [14] measured mean free paths on disordered assemblies of polystyrene spheres (so-called photonic glasses) by means of total transmission and also performed model calculations. They observe that the transport mean free path increases with wavelength. This trend agrees with our results, even though the systems are fairly different, as García *et al.* study a high density of monodisperse scatterers with a low index contrast whereas we study a low density of polydisperse particles with a high index contrast. Surprisingly, the mean free paths calculated with their model show an opposite trend with wavelength: the model predicts values from 1.8 to 1.2 μm, whereas the experiments results run from 2.3 to 3.2 μm. At this time, no reason for the opposing trends is known.

Thirdly, it was reported that broadband mean free path measurements of $TiO_2$ pigment (without polymer) by enhanced backscatter cones [15]. These results show that the mean free path increases by about a factor of 2 at wavelengths between 600 and 800 nm, in agreement with our results. Unfortunately, the results were not modeled. In their study, the mean free path was about $\ell = 1$ μm or about 100 times smaller than in our case, which can be understood by considering the density of $TiO_2$ scatterers which, in [15], are quoted on the order of 50 vol. %, about 150× more than in our experiment, which agrees with the linear scaling of scattering strength with density discussed above.

## 6. Summary and Outlook

We have studied the optical properties of diffuser slabs relevant for Fortimo white LED modules. To this end, we have measured the diffuse transmission and reflectivity over broad wavelength ranges. By employing photonic diffusion theory, we have obtained the transport mean free path that fundamentally characterizes the diffuse transport of light in such diffuser plates. To interpret our results, we have made an analytical model without freely adjustable parameters, by combining Mie theory, using the known properties of the samples, with inhomogeneous broadening as a result of the size distribution of the scattering particles. In a first model, we have averaged the relevant scattering cross sections over the whole hydrodynamic size distribution of scattering particles. The results of this model differ substantially from the observations, since the large scatterers appear to consist of clusters of smaller ones. In a second model, we have limited the size distribution to radii of individual particles that are observed by electron microscopy within large clusters. The results of this second model are a dramatic improvement over the first model. The second model agrees within 35% of the observations, and thus form a first successful *ab initio* model of diffuse light transport in a LED diffuser.

It is clear that additional work is warranted to robustly model the optical properties of diffusers for white LED modules that contain scatterers with a very broad size distribution from *ab initio*. This situation is similar to the challenge in condensed matter physics to model charge transport in the presence of a very broad inhomogeneous distribution [35,36]. Therefore, we recommend that future studies of LED diffusers be done on materials that contain scatterers with well-defined sizes and shapes. Indeed the results of [14,37] confirm that excellent diffuse optical properties are obtained by employing mixtures of size-monodisperse polymer nanospheres (see [21]) with an intentional variation in diameters. In parallel, it has been observed that samples with relatively narrow size polydispersity also yield good diffuse optical properties; in addition, these results can be successfully modeled from *ab initio* [38]. The use of high-quality nanospheres will also serve to avoid

possible challenges associated with a variation of shapes that is also apparent from the SEM in Fig. 1.

We thank Hannie van den Broek for taking the SEM pictures, and Jacopo Bertolotti, Timmo van der Beek, Otto Muskens for discussions. This work was supported by the Dutch Technology Foundation STW (contract no. 11985), and by FOM and NWO, and the ERC.

### References and Notes

1. E. F. Schubert, *Light Emitting Diodes* (Cambridge University, 2006).
2. M. R. Krames, O. B. Shchekin, R. Mueller-Mach, G. O. Mueller, L. Zhou, G. Harbers, and M. G. Craford, "Status and future of high-power light-emitting diodes for solid-state lighting," J. Display Technology **3**, 160–175 (2007).
3. H. Bechtel, P. Schmidt, W. Busselt, and B. S. Schreinemacher, "Lumiramic new phosphor technology for high performance solid state light sources," Proc. SPIE **7058**, 70580E (2008).
4. C. Sommer, J. R. Krenn, P. Hartmann, P. Pachler, M. Schweighart, S. Tasch, and F. P. Wenzl, "Effect of phosphor particle sizes on the angular homogeneity of phosphor-converted high-power white LED light sources," IEEE J. Sel. Top. Quantum Electron. **15**, 1181–1188 (2009).
5. C. Gilray and I. Lewin, "Monte Carlo techniques for the design of illumination optics," in *Illuminating Engineering Soc North America (IESNA) Annual Conference Technical Papers* (IESNA, 1996), Paper no. 85, pp. 65–80.
6. W. Cassarly, "Nonimaging optics: concentration and illumination," in *Handbook of Optics*, M. Bass, J. M. Enoch, E. W. van Stryland, and W. L. Wolfe, eds. 2nd ed. (McGraw-Hill, 2001), Vol. **3**, p. 20.
7. Z. Liu, S. Liu, K. Wang, and X. Luo, "Measurement and numerical studies of optical properties of YAG:Ce phosphor for white light-emitting diode packaging," Appl. Opt. **49**, 247–257 (2010).
8. T. W. Tukker, "Fluorescence modeling in remote and close LED illumination devices," in *SPIE International Optical Design Conference 2010* (SPIE, 2010), Paper no. ITuE2.
9. A. Lagendijk and B. A. van Tiggelen, "Resonant multiple scattering of light," Phys. Rep. **270**, 143–215 (1996).
10. M. C. W. van Rossum and T. M. Nieuwenhuizen, "Multiple scattering of classical waves: microscopy, mesoscopy, and diffusion," Rev. Mod. Phys. **71**, 313–371 (1999).
11. B. P. J. Bret, Multiple light scattering in porous gallium phosphide, Ph.D. thesis (University of Twente, 2005).
12. E. Akkermans and G. Montambaux, *Mesoscopic Physics of Electrons and Photons* (Cambridge University, 2007).
13. J. G. Rivas, R. Sprik, C. M. Soukoulis, K. Busch, and A. Lagendijk, "Optical transmission through strong scattering and highly polydisperse media," Europhys. Lett. **48**, 22–28 (1999).
14. P. D. García, R. Sapienza, J. Bertolotti, M. D. Martín, A. Blanco, A. Altube, L. Viña, D. S. Wiersma, and C. López, "Resonant light transport through Mie modes in photonic glasses," Phys. Rev. A **78**, 023823 (2008).
15. O. L. Muskens and A. Lagendijk, "Broadband enhanced backscattering spectroscopy of strongly scattering media," Opt. Express **16**, 1222–1231 (2008).
16. See catalog at: www.lighting.philips.co.uk/pwc_li/gb_en/subsites/oem/fortimo-led-catalogue/files/assets/downloads/files/Fortimo-LED-catalogue.pdf, retrieved April, 2012.
17. D. J. Durian, "Influence of boundary reflection and refraction on diffusive photon transport," Phys. Rev. E **50**, 857–866 (1994).
18. From: www.theplasticshop.co.uk/plastic_technical_data_sheets/lexan_polycarbonate_9030_technical_properties_data_sheet.pdf, retrieved May, 2011.
19. From: www.azom.com/article.aspx?ArticleID=1179, retrieved May, 2011.
20. L. Bechger, A. F. Koenderink, and W. L. Vos, "Emission spectra and lifetimes of R6G dye on silica-coated titania powder," Langmuir **18**, 2444–2447 (2002).
21. R. J. Hunter, *Foundations of Colloid Science* (Clarendon, 1993).
22. From the change and prominence of the 676 nm feature at constant $TiO_2$ density and sample thickness, we conclude that it is neither related to $TiO_2$ nor to the polymer matrix itself, but probably to unknown additives.
23. M. B. van der Mark, M. P. van Albada, and A. Lagendijk, "Light scattering in strongly scattering media: multiple scattering and weak localization," Phys. Rev. B **37**, 3575–3592 (1988).
24. J. Bartels, R. Bechmann, A. Eucken, A. M. Hellwege, and K. H. Hellwege, eds., *Landolt-Börnstein, Zahlenwerte und funktionen, Optische Konstanten* (Springer-Verlag, 1962), Vol. **2**, Part 8.
25. W. L. Bond, "Measurement of the refractive indices of several crystals," J. Appl. Phys. **36**, 1674–1677 (1965).
26. A. Lagendijk, R. Vreeker, and P. de Vries, "Influence of internal reflection on diffusive transport in strongly scattering media," Phys. Lett. A **136**, 81–88 (1989).
27. J. X. Zhu, D. J. Pine, and D. A. Weitz, "Internal reflection of diffusive light in random media," Phys. Rev. A **44**, 3948–3959 (1991).
28. H. C. van de Hulst, *Light Scattering by Small Particles* (Dover, 1957).
29. C. F. Bohren and D. R. Huffmann, *Absorption and Scattering of Light by Small Particles* (Wiley, 1983).
30. See: www.philiplaven.com/mieplot.htm, retrieved multiple instances since 2010. As mentioned on the website: "MiePlot was originally designed to provide a simple interface (for PCs using Microsoft Windows) to the classic BHMIE algorithm for Mie scattering from a sphere—as published by Bohren and Huffmann [29]".
31. K. Ishida, I. Mituishi, Y. Hattori, and S. Nunoue, "A revised Kubelka-Munk theory for spectral simulation of phosphor-based white light-emitting diodes," Appl. Phys. Lett. **93**, 241910 (2008).
32. F. Kuik, J. F. de Haan, and J. W. Hovenier, "Benchmark results for single scattering by spheroids," J. Quant. Spectrosc. Radiat. Transfer **47**, 477–489 (1992).
33. M. I. Mishchenko, "Light scattering by size-shape distributions of randomly oriented axially symmetric particles of a size comparable to a wavelength," Appl. Opt. **32**, 4652–4666 (1993).
34. While performing computations of Eqs. (8)–(10) with a size distribution cutoff at $R = R_{\max}$, we have carefully applied proper normalization. Thus the denominator of the equations was also integrated from $R = 0$ to $R = R_{\max}$ to obtain the proper total number density of scatterers $n \equiv (N/V)$.
35. A. Lagendijk, in *Ultrashort Processes in Condensed Matter*, W. E. Bron, ed. (Plenum, 1993), pp. 197–238.
36. X. H. Yan, J. W. Ding, and Q. B. Yang, "Size and randomness effects on the temperature-dependent hopping conductivity of nanocrystalline chains," Eur. Phys. J. B **20**, 157–163 (2001).
37. M. D. Birowosuto, S. E. Skipetrov, W. L. Vos, and A. P. Mosk, "Observation of spatial fluctuations of the local density of states in random photonic media," Phys. Rev. Lett. **105**, 013904 (2010).
38. A. F. Koenderink, A. Lagendijk, and W. L. Vos, "Optical extinction due to intrinsic structural variations of photonic crystals," Phys. Rev. B **72**, 153102 (2005).